Reconstructing the Hyshot flights

T Cain
Gas Dynamics Ltd.,
2 Clockhouse Road, Farnborough, GU14 7QY
Hampshire, UK

tcain@gasdynamics.co.uk

ABSTRACT

The first and second University of Queensland's Hyshot flights are reconstructed from on-board sensor data. It is shown that Hyshot-1 failed due to roll-pitch coupling during launch and that perhaps Hyshot-2 was lucky to escape the same fate. Techniques are demonstrated that made it possible to determine the vehicles altitude, attitude and speed throughout the successful Hyshot-2 flight, from a relatively limited set of sensors.

1 INTRODUCTION

The University of Queensland's Hyshot programme has the objective of obtaining supersonic combustion data in flight at high Mach number for comparison with those obtained in shock tunnels. The first flight, Hyshot-1, took place on the 30th October 2001 and the second, Hyshot-2, on the 30th July 2002. Aerodynamic data were obtained during both flights but it was only on the second that the supersonic combustor was tested. This programme was the first experience of flight testing for many of the individuals involved and the launch failure of the first flight and subsequent successful Hyshot-2 is a tale of innovation and perseverance best told by the lead partner.

The author's contributions to these flights were mostly concerned with the vehicle aerodynamics and trajectory during reentry [1, 2] and in this lecture these problems are revisited and a previously published analysis is explained and refined. Reconstructing the flight was made more difficult by the lack of: radar or GPS data to provide velocity and position; or inertial system to provide attitude; or rate gyroscopes to provide angular rates. Altitude, velocity, and attitude were all derived from measurements by pressure sensors, accelerometers, a magnetometer and an horizon sensor. Fortunately these transducers were sufficient to provide a complete picture of the flight and it is the techniques that were developed for determining the vehicle state from these indirect measurements that are the primary focus of this lecture. Attention is also given to the Hyshot-1 failure which appears to have been due to roll-pitch resonance. There is much to be learnt from Hyshot's hard introduction to this classical sounding rocket problem.

2 THE HYSHOT TEST TECHNIQUE

The scramjet was mounted on the tip of a two stage-sounding rocket, figure 1, but was covered by a standard 3:1 ogive nose cone during launch. The nose cone protected the copper heat-sink scramjet from warming during ascent and more importantly it preserved the sounding rocket's established aerodynamic characteristics in the launch phase. The two-stage sounding rocket consists of a Terrier MK-70 motor that burns for 6s accelerating an Improved-Orion second stage to approximately Mach 3.6. After a short coast phase the Orion-5A motor is ignited and it burns for 25s while accelerating to 2.37km/s. The nosecone is ejected at an altitude above 100km and the spent rocket continues to climb to an apogee of approximately 330km before falling back to earth. The scramjet remains attached to the Orion for the entire flight and in this exposed configuration the vehicle is known as the UQ-Orion. The UQ-Orion re-enters the atmosphere after approximately 8 minutes in space and the scramjet test begins 20s later when the dynamic pressure is approximately 25kPa.

Figure 1: The UQ scramjet mounted on the Terrier Orion sounding rocket. Photo: Chris Stacey, The University of Queensland

The attractions of the Hyshot test technique are apparent from the Mach-number/dynamic-pressure chart of the Hyshot 2 trajectory presented in figure 2. The launch rail was set at 77° from the horizontal to enable the rocket to accelerate in the upper atmosphere, minimising the energy loss due to drag. By the time the vehicle has been accelerated to Mach 7.2 it is at an altitude of 52km and the dynamic pressure (2kPa) is too low for scramjet operation. However near the end of the flight when the vehicle is descending back through the atmosphere it traverses the airbreathing corridor (dynamic pressure from 0.25 to 2bar) at a nearly constant Mach number of 7.6.

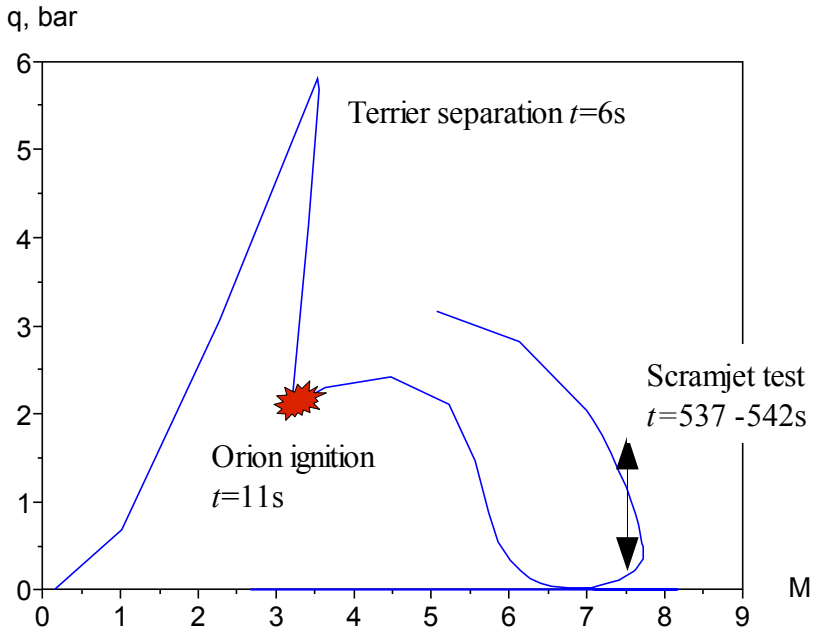

Figure 2: The Hyshot strategy for obtaining the right combination of Mach number and dynamic pressure

In order that the scramjet is at an angle of attack of less than 4° during the test (the limit for the UQ intake) the vehicle must enter the atmosphere at an angle of attack less than about 30° and this requires an attitude adjustment in space. Without this manoeuvre to align the vehicle axis with the re-entry velocity vector the spinning UQ-Orion would enter the atmosphere almost tail first, at an angle of attack of 140°. The realignment is complicated by the fact that the vehicle is spinning at 5.3Hz. This spin is induced by canting the Orion fins at approximately 0.5° and is applied to ensure that any rocket thrust misalignment is averaged out during the ascent, and hence will not result in a large deviation from the planned flight path. The spin is *not* sufficient to gyroscopically stabilise the vehicle except at very low dynamic pressure. The Orion is kept at small angles of attack during ascent by virtue of its aerodynamic stability created by the large tail fins. The natural frequency of the weathercock pitching motion due to this aerodynamic stability varies with Mach number and dynamic pressure. When it coincides with the frequency that the vehicle is spinning, the resonance can lead to a catastrophic increase in angle of attack and it is very likely that Hyshot-1 suffered this fate, as will be demonstrated.

Once in space there are are no aerodynamic forces and an attitude control system is needed in order to align the vehicle axis with the velocity vector. UQ designed and built a system based on a cold gas (nitrogen) thruster with a fast acting valve. Correct valve timing was determined using feedback from an horizon sensor and a 3-axis magnetometer. The functioning of the system in Hyshot-2 is discussed in more detail later as it was necessary to model the system in order to obtain the UQ-Orion attitude at re-entry.

3 AXIS SYSTEM AND NOTATION

Well defined axes systems considerably reduce the uncertainty and workload in preparing conducting and analysing a flight test. Unfortunately a single axes system is not convenient for all purposes and within this paper five different coordinate systems are used:

- A right handed *Inertial* axes system X, Y, Z with origin at the centre of the earth. The Z axis is aligned with the polar axis and positive north, while X and Y are in the equatorial plane. X passes through the longitude of the launch point at launch (t=0), but remains fixed in space as the earth rotates.

- A right handed *Body* axes system x, y, z with origin at the centre of gravity of the UQ-Orion. The x axis is positive towards the nose and y is positive to starboard. Figure 3 is a cross sectional view through the UQ-Orion looking forward along this x-axis and contains the key features required for orientation. The body attitude is defined in the inertial system by the Euler angles. These are the rotations that would be required to align X, Y, Z with x, y, z and are made in the order beginning with a rotation about Z, then rotating about the carried Y and finally rotating about the carried X. All rotations are positive clockwise.

- A right handed *Gravity* axes system X', Y', Z' with origin at the centre of the earth that serves as an intermediate axes between the inertial and body-axes systems. The X' axis of this system passes through the origin of the body-axes at all times, and Z' is due north while Y' is due east. The vehicle latitude, α, and longitude, β, are defined by the rotations that would be required to align X, Y, Z with X', Y', Z'. (That is, β-β_X about Z followed by -α about the carried Y.) The vehicle Heading, ψ, pitch, θ, and roll, ϕ, are defined by the rotations that would be required to align X', Y', Z' with x, y, z. (That is, -ψ about X' followed by θ-$\pi/2$ about the carried Y' followed by ϕ about the carried X'.)

- A right handed *Wind-tunnel* axes system x_w, y_w, z_w with origin at the centre of gravity of the UQ-Orion is used to define the aerodynamic data. The x_w axis is aligned with the vehicle axis and positive rearwards and z is orientated so that the free stream velocity vector is always in the x_w-z_w plane. A positive angle of attack corresponds to a positive rotation about y_w. Moments about x_w, y_w

and z_w are L_w, M_w and N_w respectively and rotation rates are p_w, q_w, and r_w respectively. The aerodynamic forces are normalised by the base area of the Orion, A_b, and the dynamic pressure, Q. The reference length for moment coefficients is the Orion diameter, d.

- A two dimensional *Natural* coordinate system with an origin at the centre of the earth. In this system the vehicle is treated as a point mass a distance r from the centre of the earth, with a velocity V at an angle γ to the horizon (the flight path angle). This coordinate system is particularly suited to determining altitude and speed from measured accelerations.

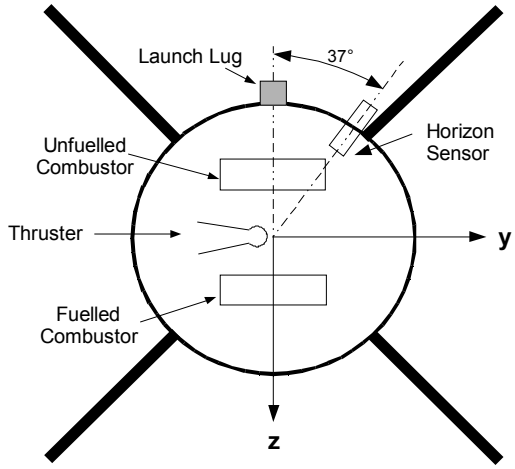

Figure 3: The UQ payload viewed from behind along *x*.

4 THE LAUNCH PHASE

4.1 Hyshot-1 launch anomaly

Axial acceleration measured during the Hyshot-1 launch is plotted in figure 4. The initial 6s of high acceleration are during the Terrier burn, then there is a 5.5s coast phase before the Orion ignites. The Orion motor has boost and sustain phases, as evident by the transition to low acceleration that occurs at about t=16s. However the acceleration during the sustain phase is unusually low and the reason for this becomes clear at burnout (t=33s) when the declaration due to high aerodynamic force is apparent. The Orion was at high angle of attack and its corkscrew trajectory is obvious from the smoke trail photographed from the ground (figure 4).

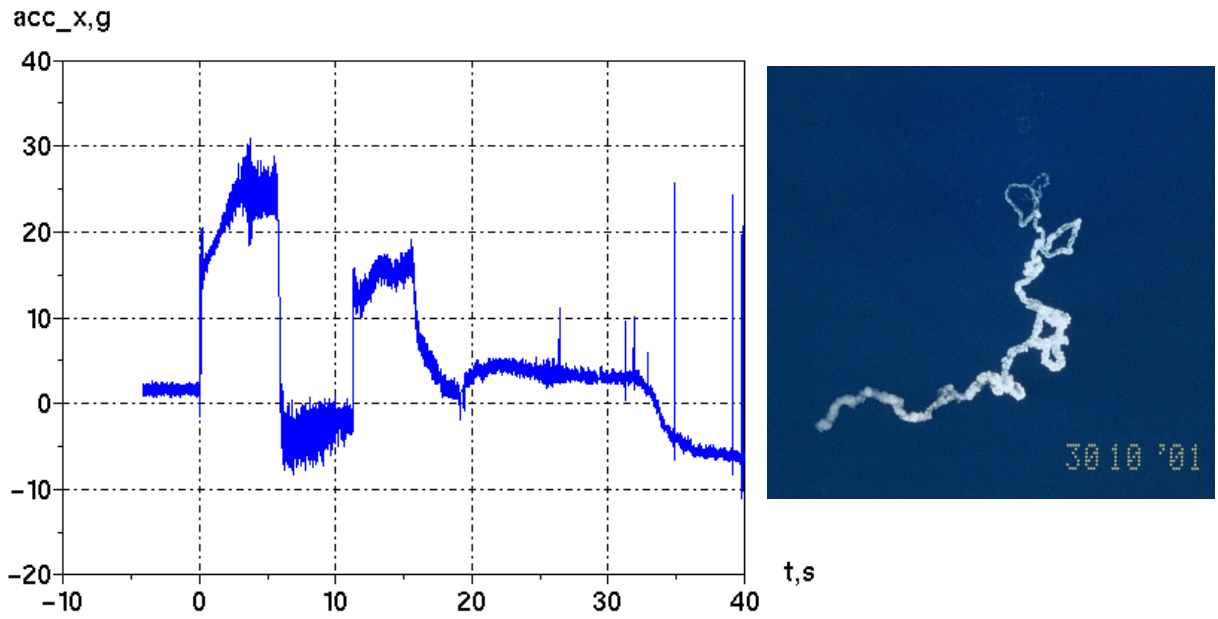

Figure 4: Axial acceleration measured during Hyshot-1 and the Orion smoke trail photograph courtesy of T. H. Cain , spectator.

An enquiry into the launch anomaly concluded that it was most likely the result of failure of the Nike fins fitted to the Terrier, putting the Orion in an attitude at separation from which it could not recover [3]. However a comparison of the Hyshot-1 y, z accelerometer signals with those from the successful Hyshot-2 tells another story. This comparison is made after a brief introduction to the roll-pitch resonance phenomenon.

4.2 Roll-Pitch resonance

The response of the Orion to a pitching moment M and a yawing moment N is given by [4],

$$M = \dot{q} I_{yy} + p r (I_{xx} - I_{zz}) \quad \text{and} \quad N = \dot{r} I_{zz} + p q (I_{yy} - I_{xx}) \qquad [1]$$

where p, q and r are the angular rates about x, y and z and the moments of inertia in pitch and yaw (I_{yy} and I_{zz}) are very much greater than that in roll (I_{xx}). An appreciation of the resonance phenomenon can be gained by first considering only planar pitching motion. In this case the tail fins help to generate an aerodynamic moment M that opposes an increase in angle of attack, σ, that is essentially proportional to σ. The result is simple harmonic motion about σ=0 at the weathercock frequency given by,

$$\omega_c = \sqrt{\frac{M}{I_{yy}\sigma}} \qquad [2]$$

If in addition to M there is a pitch trim moment, perhaps due to rocket thrust misalignment or an asymmetry in the vehicles construction, then the response is simple harmonic oscillation about the trim angle of attack. However if the body is spinning at a rate $p=\omega_c$ then the trim vector has rotated through 90° when the pitch is near maximum amplitude, and through 180° as the body swings back through zero incidence. Figure 5 is a linear representation of angular planar motion and can be thought of as a view of the base of the rocket oscillating about the velocity vector, which is normal to the page and on the horizontal line. At this resonant condition the trim moment is in phase with the angular velocity and hence

the energy and amplitude of the oscillation grow with each swing. In the three dimensional case, the rotating trim vector also excites angular motion normal to the plane which we have been considering, and the result is a spiralling increase in total angle of attack with the trim moment at 90° to the restoring aerodynamic moment.

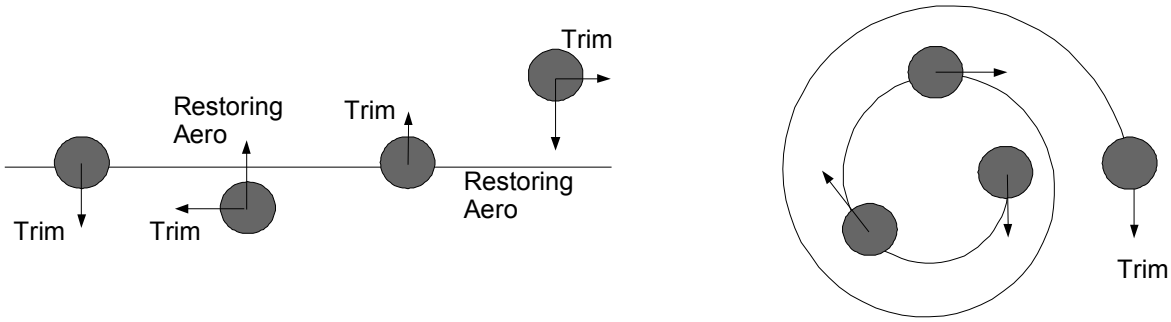

Figure 5: Schematic of roll-pitch resonance

4.3 Quantitative interpretation of the *y* and *z* accelerometer signals

The above simplified description of roll-pitch resonance is difficult to reconcile with equation 1 in which the angular rates are referred to body coordinates. However this coordinate system is convenient for interpretation of the onboard accelerometers. The *y* and *z* accelerometers were located a distance x_a ahead of the centre of gravity. Therefore [4],

$$a_y(x_a)=a_y(0)+(pq+\dot{r})x_a \quad \text{and} \quad a_z(x_a)=a_z(0)+(pr-\dot{q})x_a \qquad [3]$$

Noting that $I_{yy}\approx I_{zz}$ and $I_{yy}>>I_{xx}$, equation 1 can be substituted into equation 3 to give,

$$a_y(x)\approx a_y(0)+\frac{N x_a}{I_{zz}} \quad \text{and} \quad a_z(x)\approx a_z(0)-\frac{M x_a}{I_{yy}} \qquad [4]$$

An alternative form is derived by substitution of: $I_{yy}=I_{zz}=mk^2$, $N=F_y x_{cp}$ and $M=-F_z x_{cp}$ to give,

$$a_y(x)\approx \frac{F_y}{m}\left(1+\frac{x_a x_{cp}}{k^2}\right) \quad \text{and} \quad a_z(x)\approx \frac{F_z}{m}\left(1+\frac{x_a x_{cp}}{k^2}\right) \qquad [5]$$

where: *m* is the vehicle mass, *k* is its longitudinal radius of gyration and x_{cp} is the centre of pressure.

Equation 5 tells us that angular rates do not significantly affect the accelerometer outputs and hence even though they were not located at the centre of gravity, they can provide an indication of the Normal forces, F_y and F_z and therefore of the crossflow direction. However, the phase calculation is particularly sensitive to offset errors when the acceleration levels are low. These offsets can arise from a bias on the Analogue to Digital conversion, or geometric offsets ($y_a\neq 0$, $z_a\neq 0$, and angular misalignment) that result in sensitivity to angular and linear accelerations that are not accounted for in equation 5. The *y*, *z* accelerometer signals outputs from the two flights that are presented in figure 5 have been corrected for these sensitivities and offsets. The corrections are made by comparison with other phases of the flight in which the vehicles state is known, for example on the launch rail and in space, and although they are important, the details of the corrections are too tedious to include here.

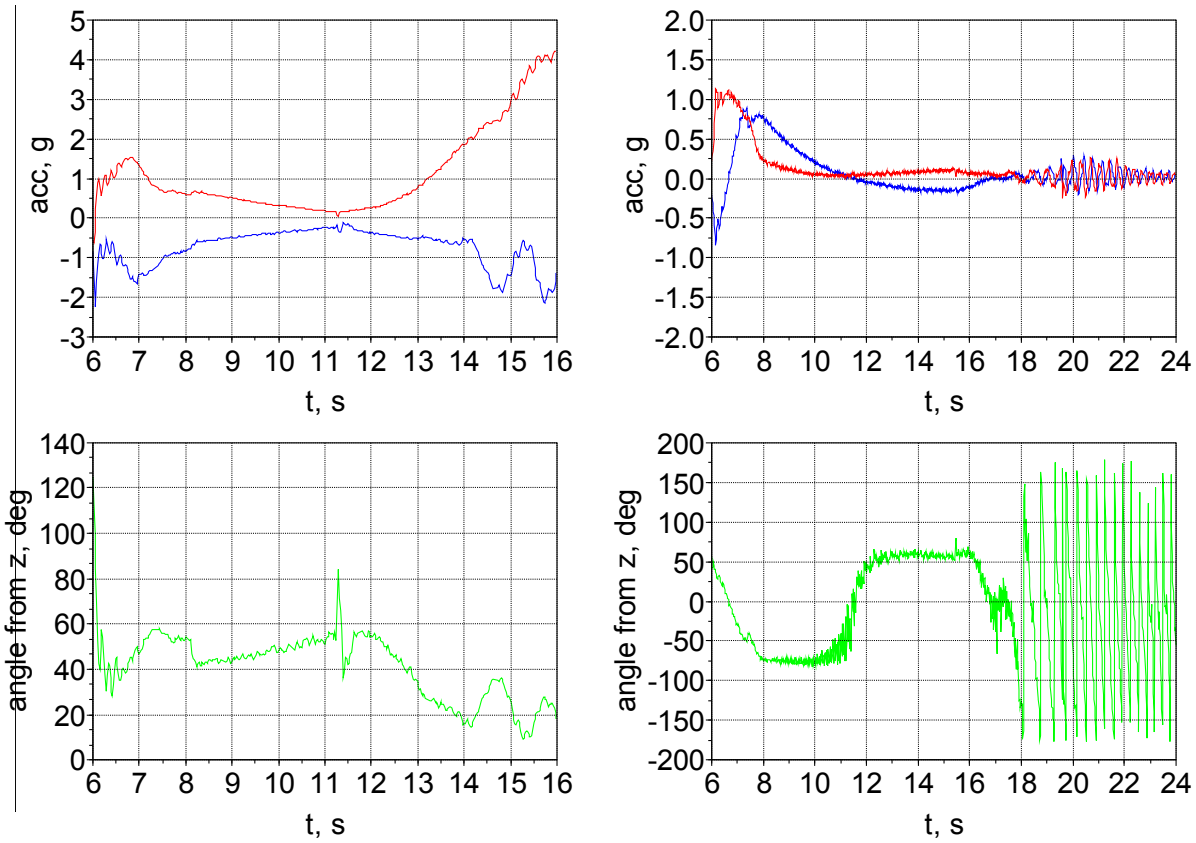

Figure 6: Measured y (green line), z (red line) accelerations in Hyshot-1 (left) and Hyshot-2 (right)

At the end of boost (t=6s) the magnitude and phase of the acceleration is the same for both flights. Hence there is no evidence of an untidy or difficult separation in Hyshot-1. In both flights the Orion is spinning at approximately 3Hz during the coast phase and yet the aerodynamic Normal force does not rotate around the body. The vehicles are pitching at the spin frequency and the fin located 45° clockwise from z (figure 3) remains in the lee for the entire coast phase. Orion ignition occurs at t=11.3s in Hyshot-1 and the magnitude of the Normal acceleration rapidly but steadily increases; providing no evidence of a gross misalignment in thrust but a clear indication that angle of attack is steadily increasing. During the next 4.5s the Normal force vector rotates through only ≈30° relative to the body which itself has spun through >4500°. The resonance was not transient, roll had locked onto pitch and the canted fins did not provide sufficient torque to escape this catastrophic predicament.

Orion ignition was delayed until t=15.4s in Hyshot-2 but roll remained locked to Pitch during the extended coast. The Orion did rock from one orientation to another (≈+50° to ≈-75° to ≈+60°) but at ignition the crossflow had practically the same orientation as for Hyshot-1. The response to the increasing speed and dynamic pressure following ignition was very different. In Hyshot-2 the Orion breaks free of the lock-in and begins to spin up. For the remainder of the ascent the crossflow vector rotates around the Orion at a frequency corresponding to the difference between spin and weathercock frequency.

The significant difference between Hyshot-1 and 2, is the increase in magnitude of the z acceleration following ignition. The lower altitude with corresponding higher dynamic pressure would have contributed to the rate of amplification in angle of attack in Hyshot-1 but perhaps the failure of one and the success of the other can be attributed to nothing more than the random alignment of the trim moment (produced by the motor) with the crossflow vector.

4.4 Altitude and velocity from axial acceleration

Natural coordinates are the most convenient when determining the flight path from measured axial acceleration, a_x. For the ascent it is assumed that the vehicle is at small incidence and therefore the acceleration along the velocity vector, $a_V=a_x$. With velocity, local gravity, flight path angle, and radius from the centre of the earth represented by V, g, γ and r respectively,

$$V = V_1 + \int_{t_1}^{t_2} (g \sin\gamma + a_V)\, dt \qquad [6]$$

$$\gamma = \gamma_1 + \int_{t_1}^{t_2} \left(\frac{V}{r} - \frac{g}{V}\right) \cos\gamma \, dt \qquad [7]$$

$$r = r_1 + \int_{t_1}^{t_2} V \sin\gamma \, dt \qquad [8]$$

Simultaneous integration of the above equations is used to to determine the vehicles state during ascent. Note that wind and the rotation of the earth are neglected and this makes the results insufficiently accurate to determine the impact point. The method is used here to calculate velocity and dynamic pressure during ascent.

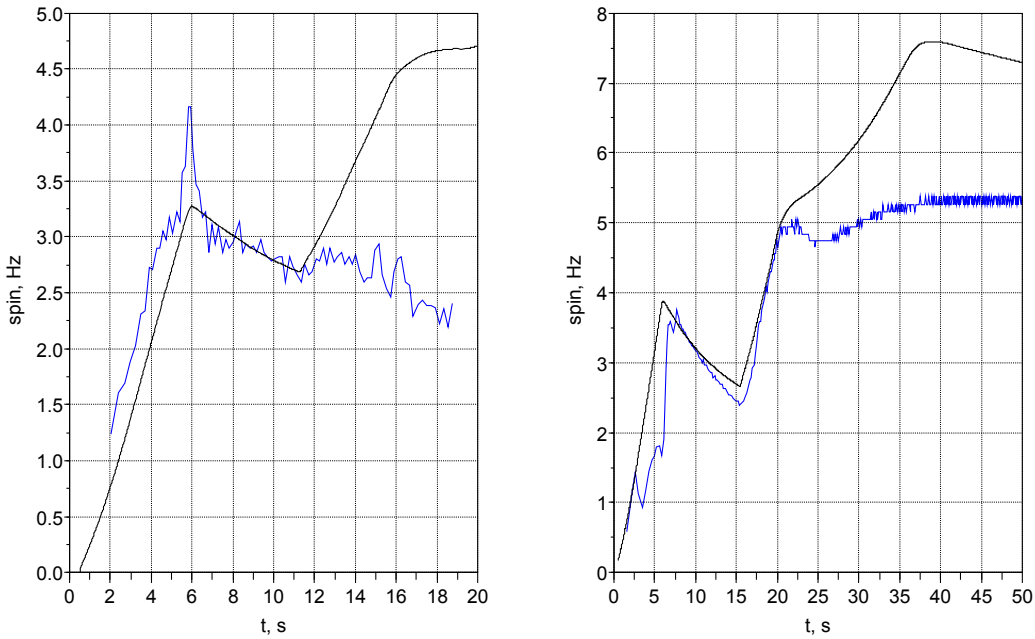

Figure 7: Measured and 'expected' spin rates in Hyshot-1 (left) and Hyshot-2 (right)

The fins of the Orion are canted (set to a small angle of attack) so that a net torque is developed until it is spinning at a rate in which the effective angle of attack on the fins is just sufficient to balance the viscous torque acting on the body. In effect this results in a spin rate nearly proportional to velocity and the Orion screws itself clockwise into the sky with a pitch of about 3 turns every kilometre. Figure 6 is a plot of the spin rate expected if it were proportional to velocity and for comparison, the spin measured from the

cycles detected by the *y*-magnetometer. The Hyshot-1 result clearly shows how spin remained locked to the weathercock frequency. For Hyshot-2, spin is seen to recover to the expected value soon after ignition but departs again some 4s later as the motor makes the transition from boost to sustain phase. Dynamic pressure is about 1.5bar at this time and the velocity is 1.5km/s. The author does not know the reason for the departure, it may be an aero-elastic phenomenon, whatever the cause it is normal for the Orion which achieved the desired spin rate (5.3Hz) on this flight.

5 HYSHOT-2 EXOATMOSPHERIC FLIGHT

5.1 Pitch and Roll from the horizon sensor

Once the Orion left the atmosphere its nose cone was ejected and the horizon sensor underneath detected the sunlight reflected by the earth. Figure 8 shows the output of this simple photo diode mounted at the bottom of a long hole. The hole was drilled 217° clockwise from *z*, figure 3, and at an angle ε=14° from the *y*-*z* plane as shown in figure 8. Output is high as the receptor beam (line AB, figure 8) sweeps across the earth but for the remainder of the UQ-Orion roll, the beam receives very little light from space and the signal is low. Direct light from the sun can confuse the picture in some attitudes.

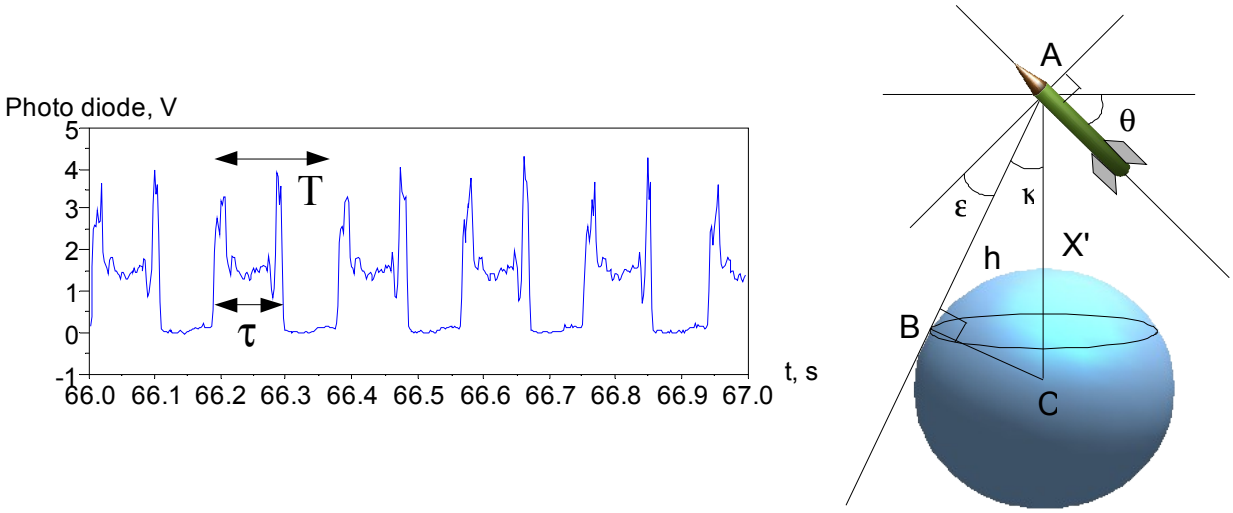

Figure 8: Horizon sensor signal interpretation

The middle of the light plateau corresponds to a roll angle of 180-37=143° (figure 3) since the sensor then is pointing directly between the horizons. Pitch, θ, is also measured by the sensor as the Mark-Space ratio of the High-Low signal depends on pitch. Letting 2ϕ be the difference in roll angle from one horizon to the other; and T and τ be as defined in figure 8, then,

$$\frac{\tau}{T}=\frac{2\phi}{2\pi} \qquad [9]$$

The semi infinite line that is the extended AB (representing the receptor beam), is tangent to the earth's surface (the horizon) at a distance h from the sensor when,

$$h\cos\kappa = h\sin\epsilon\sin\theta + h\cos\epsilon\cos\theta\cos\phi \qquad [10]$$

Equation 10 was written as a quadratic in $\cos\theta$ and solved as a function of the measured ϕ and the angle κ, which was determined from the lengths AC and BC. AC is the distance of the UQ-Orion from the centre of the earth and BC is nominally the earth's radius, R_0. However since the atmosphere also reflects

sunlight, BC is greater than R_0 by the height of the earth's "Limb". The Limb height depends on many factors not least of which is the sensor's response characteristic. Here it is taken as 40km as this gives a good match to the flight path angle prior to the attitude control manoeuvre as shown in figure 9.

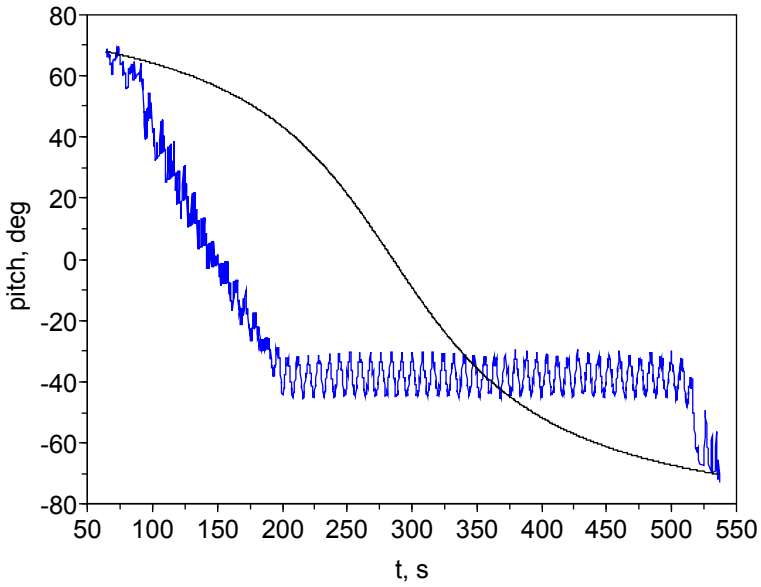

Figure 9: Calculated flight path angle (black) and measured-pitch (blue) in Hyshot-2

Flight path angle can be calculated by simultaneous integration of equations 6 to 8 with a_v=0, if the easterly component of velocity imparted by the earth's rotation is added to the velocity vector calculated at the end of the launch phase (t=64.4s, altitude=106.6km). However conservation of energy and momentum in the inertial frame, in conjunction with the inverse square law for gravity, enable an analytical solution for the exoatmospheric flight and Kepler's equations are used for this phase of the flight as demonstrated in a previous paper [2]. There are many references on orbital mechanics available so those equations are not repeated here.

5.2 The reorientation manoeuvre

The attitude control manoeuvre began at t=76s and finished at t=201s. The manoeuvre left the vehicle coning with 5.6° half-angle about an angular momentum vector, **H**, pitched 38° below the horizon (θ=-38°). The attitude control had not gone to plan, primarily because an unforeseen light path had allowed direct sunlight to unduly influence the horizon sensor. The bang-bang attitude control depended on firing the thruster while the UQ-Orion was at zero roll (and the thruster horizontal). In this way the impulse alters only the pitch of **H** and not its heading. Once the vehicle has nutated 180° around **H**, and at a time when roll is zero, the thruster is fired again so that **H** is brought back into alignment with the vehicle axis and the UQ-Orion stops coning. The bang-bang cycle is repeated as many times as necessary in order to rotate **H** (and the UQ-Orion) from θ=+70° to θ=-70° in preparation for reentry.

To generate sufficient impulse, the thruster must be fired over an arc centred about zero roll, rather than at zero roll, since that only occurs for an instant. UQ designed the system to fire over the arc -30°<ϕ<30° and figure 10 shows when it actually fired in flight, as determined from the y-accelerometer and the horizon sensor. The diamond symbols mark the roll angle at which the valve opened and the cross symbols mark when it closed. The very first pulse is used to eject the nose cone by releasing a catch and pressurising the

volume within the cone. This pulse was made blind as the horizon sensor was covered by the nose cone. The valve timing shown for this nose-blowing pulse is the part that resulted in a net *y*-force. The next seven pulses are well timed but after this the system becomes confused by the sun and switches to the magnetometer to determine roll. Unfortunately an error in this back up system resulted in all subsequent thrusts being centred about ϕ=30° and hence induced a change in heading as well as pitch.

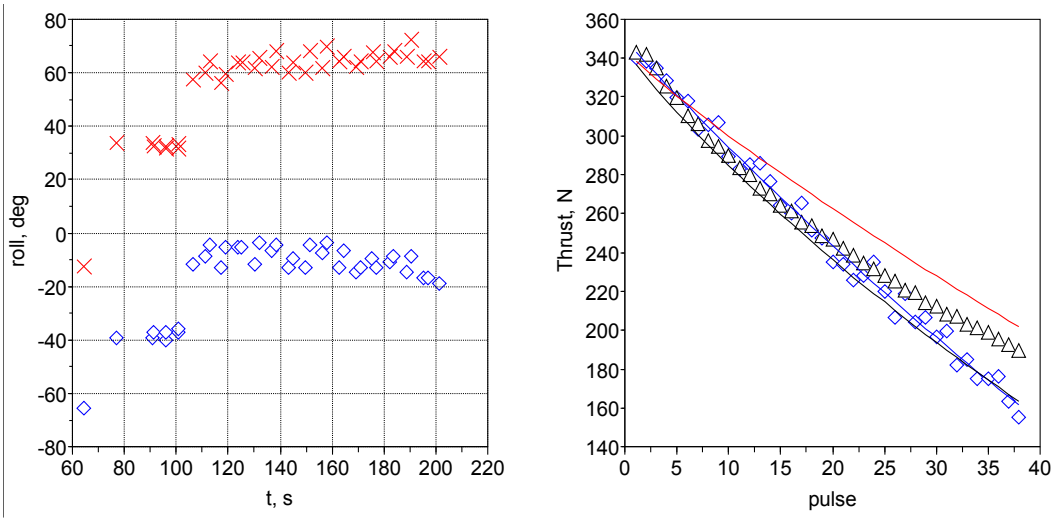

Figure 10: On the left- roll angles at valve opening (diamond) and closing (cross). On the right- the average thrust as measured by the *y*-accelerometer (diamond) and predicted from the measured nitrogen supply pressure (triangle). The red line is the predicted decrease in thrust for an isothermal nitrogen supply and the black is for adiabatic.

Magnetic interference prevented the use of the magnetometer as an independent source of heading information. So in order to determine the UQ-Orion attitude at re-entry, the reorientation manoeuvre was reconstructed from the flight data and this required a measure of the thrust during each pulse. One approach was to calculate thrust from the measured tank pressure multiplied by a thrust coefficient of 1.18 and the thruster throat area of 14.5mm^2. The thrust coefficient was calculated to match the simulated total pitch change with the measured value [2]. This empirical coefficient is 74% of the ideal (lossless) value, calculated by neglecting pressure drops in the supply line and viscous and divergence losses in the nozzle. The second approach was to calculate thrust from the measured *y*-acceleration, using equation 5, with x_{cp}=1.94m being the distance of the thruster from the UQ-Orion centre of gravity. The results of both approaches are plotted in figure 10. The scatter in the *y*-accelerometer results is due to the low resolution at acceleration levels that are only 5% of full scale. Since this error is random, the precision can be increased by curve fitting the results as shown. Significantly the fall in thrust levels, due to the drop in tank pressure, appears to follow a trend that is dependent on the choice of transducer: the *y*-accelerometer results indicate an almost linear fall with each pulse and are reasonably close to the prediction for an adiabatic supply; the tank-pressure results initially follow the adiabatic prediction but later approach the isothermal prediction. There is no reason to doubt the accelerometer result whereas the pressure transducer at the tank outlet is known to be sensitive to temperature and therefore thrust was determined from the the curve fit to the accelerometer data.

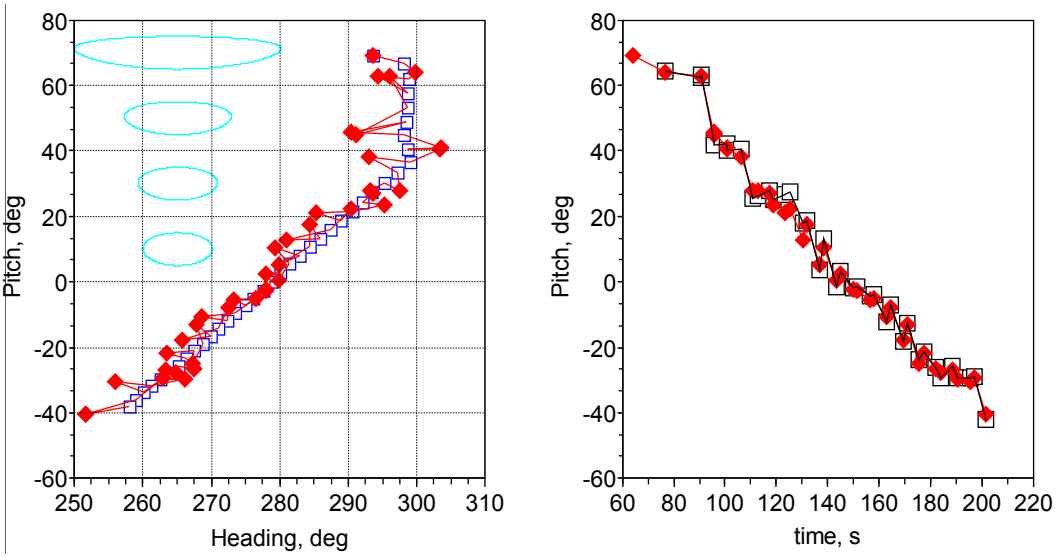

Figure 11: Simulation of the reorientation manoeuvre. On the left- mid-pulse orientation of the body (diamond) and angular momentum vector (square). On the right- calculated (diamond) and measured (square) mid-pulse body pitch.

Attitude of the angular momentum vector, **H**, is calculated by vectorial addition of the moment impulses at each thrust. Rotation matrices are used to convert the impulse from body axes to the inertial coordinate system. Initial pitch and heading; thrust timing and magnitude; nutation rate; and the UQ-Orion roll attitude are the only inputs to the calculation. The body attitude is calculated by rotating it around **H** from pulse to pulse at the measured nutation rate (45.0°/s, 30 cycles from t=240s to t=480s, figure 9).

The unforced agreement between the calculated and measured pitch is remarkable (figure 11) and gives a high degree of confidence in the calculation of the change in heading created by the manoeuvre. Mid-pulse headings of the body and **H** are presented in figure 11, revealing a 40° shift resulting from the switch from horizon sensor to magnetometer. The approximately elliptical shapes drawn on the figure trace a body nutating with a 5° cone angle and were included to explain why the nutation arms that link the body to **H**, appear to be of inconsistent length in the heading/pitch plane.

6 HYSHOT-2 RE-ENTRY

6.1 Angle of attack from ramp and Pitot pressure

The misalignment of the body axis and flight path following the partially successful reorientation resulted in moderate angles of attack during the scramjet test. Fuel injection began at t=537s and figure 12 shows Pitot pressure signals midway through the test. A Pitot probe was mounted on both the port and starboard sidewall, 143mm downstream of the intake leading edge and 35mm normal to the wall on the x-y plane of symmetry. The top and bottom mounting holes of the starboard probe are the pair closest to the leading edge in figure 1, but the fragile titanium-zirconium-molybdenum probe was not screwed into place until just before flight. At t=539.5s the UQ-Orion is spinning at approximately 6Hz and the probes are alternately placed in the shock layer formed over a leeward separation (visible in wind tunnel schlieren photographs [1]). The large spurious increases in Pitot pressure, figure 12, are due to this interference. Peaks and troughs in the ratio of pressures measured on the top and bottom intake ramps were used to identify times of zero sideslip. At these times, both probes are clear of interference but the sample window is narrow and this selection process resulted in residual noise in the data [2]. For the current analysis the

fitted Pitot signal has been constructed by alternately switching from port to starboard probe using only data from the windward side near maximum sideslip.

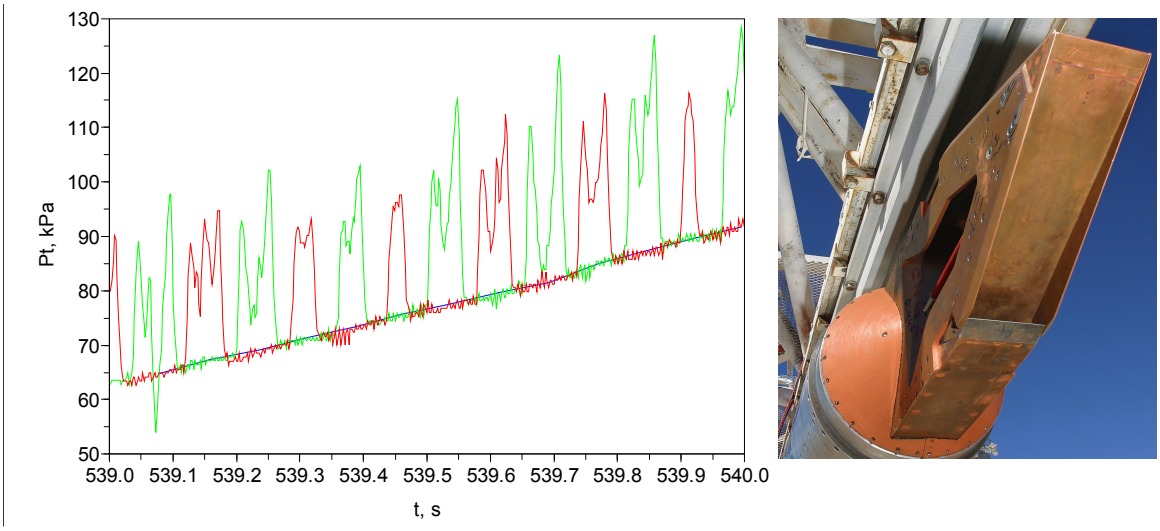

Figure 12: A one second period of the port (red) and starboard (green) pitot signals and the fitted result (blue). UQ scramjet photo: Chris Stacey, The University of Queensland.

With the clean, interpolated Pitot signal and pressure from one of the 18° intake ramps, the angle of attack, α, could be determined by taking the pressure ratio at times when sideslip was zero, and comparing it with the pressure ratio calculated for a shock induced deflection of 18°+α. In principle either ramp could have been used, or both, making Pitot pressure unnecessary. In practice the pressure measurement on the ramp of the unfuelled combustor, appeared to under-read by 4% after calibration using the vacuum of space and the atmosphere on the launch rail. This is another example of the value of redundancy created by having additional transducers or more than one method of deriving an important quantity.

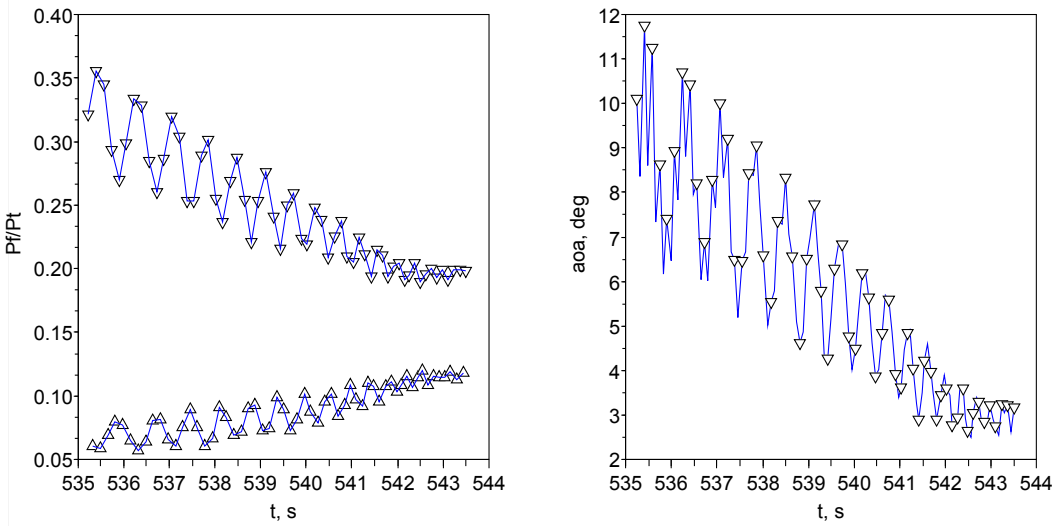

Figure 13: Total angle of attack, aoa, (right) from the ratio of pressures (left) from the fuelled-combustor-intake-ramp and Pitot probe when sideslip is zero. Inverted triangles mark positive α.

6.2 Altitude, velocity and flight path angle from Pitot pressure

At velocities of 1.8 to 2.8km/s in the stratosphere, the Pitot pressure, P_t, for air in vibrational equilibrium is very well described by,

$$P_t = 0.938\,\rho\,V^2 \qquad [11]$$

Balloon measurements of temperature and pressure taken before the flight meant that density, ρ, was known as a function of altitude. If the vehicle's velocity was also known then altitude could be determined from the Pitot measurement at any instant. Since the rate of change of altitude is just $V\sin\gamma$ the Pitot history contains enough information to determine both altitude and velocity if the flight path angle, γ, is known. In a previous publication [2] γ at any altitude was assumed to be sufficiently well predicted by the trajectory calculated from launch. Following recognition of the significance of wind on the ascent trajectory, a method to determine flight path angle as well as velocity and altitude was investigated.

The method fits Pitot pressures at altitudes from 23 to 34km in 200m steps. A guess of V at 23km allows the calculation of P_t and matching this with the flight data synchronises time, t. A guess of γ at 23km provides the remaining initial condition required for the simultaneous integration of equations 6 to 8, stepping backwards in time. Acceleration along the velocity vector, a_v, is calculated from the synchronised x-accelerometer data, a_x, through the relationship,

$$a_v = (1 + 0.1\sigma + 11.9\sigma^2)\,a_x \qquad [12]$$

Equation 12 relating Drag to axial force (and their respective accelerations) at a total angle of attack, σ (in radians), is derived from wind-tunnel data for the UQ-Orion [1].

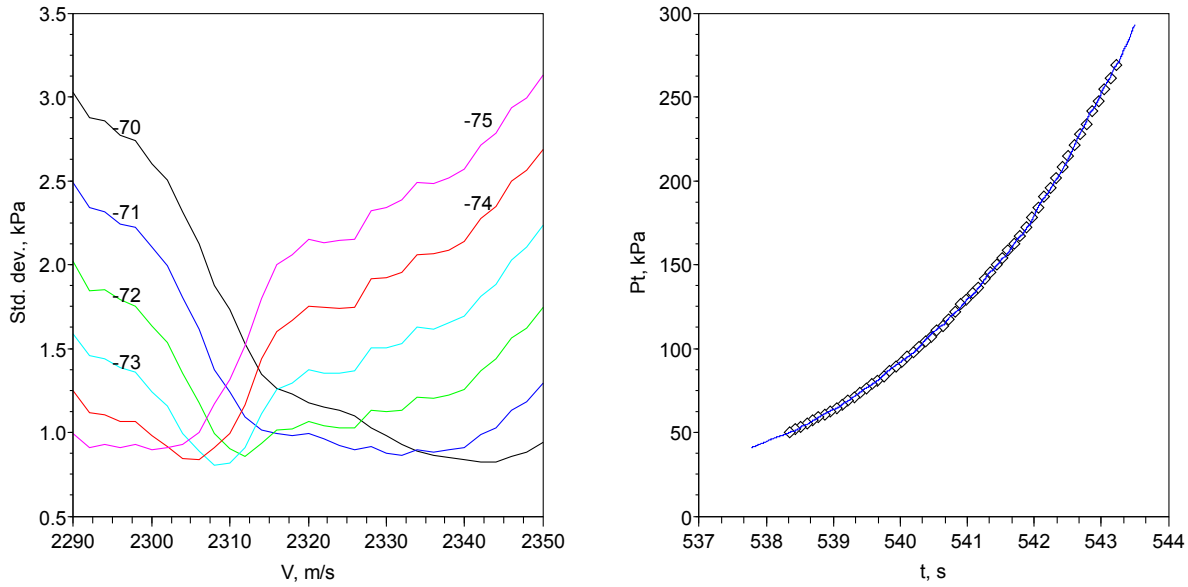

Figure 14: On the left, standard deviation of calculated from measured Pitot pressure as a function of velocity and flight path angle at an altitude of 23km. On the right a comparison of measured P_t (blue line) with that calculated (diamond) using the optimum initial condition (γ=-73°, V=2308m/s).

Standard deviation of the calculated P_t from the measured values, is determined for each guessed pair of initial conditions, γ and V. The correct pair is taken as that which results in the smallest deviation over the 23 to 34km range. Figure 14 illustrates the procedure and the optimum fit to the data corresponding to the γ=-73°, V=2308m/s initial condition. Although a very close fit to the data is demonstrated, it is in fact only marginally better than the fit for the γ=-70°, V=2342m/s initial condition. The lower deviation for the γ=-73° optimum; its symmetry; and the fact that it is expected from the nominal trajectory; all make it easier to accept this result. However, more work needs to be done to quantify and reduce the uncertainty and perhaps the key to a precise measurement of velocity is the accurately measured time of flight.

6.3 Six degree of freedom simulation

Provided one has an aerodynamic model of the vehicle, solving the equations of motion is made relatively simple by the ready availability of software for integrating ordinary differential equations, such as the open source "Scilab" used here (download from www.scilab.org). UQ-Orion mass properties and polynomial fits to the wind tunnel data were taken from a previous publication [1] and initial conditions for the re-entry were as defined above.

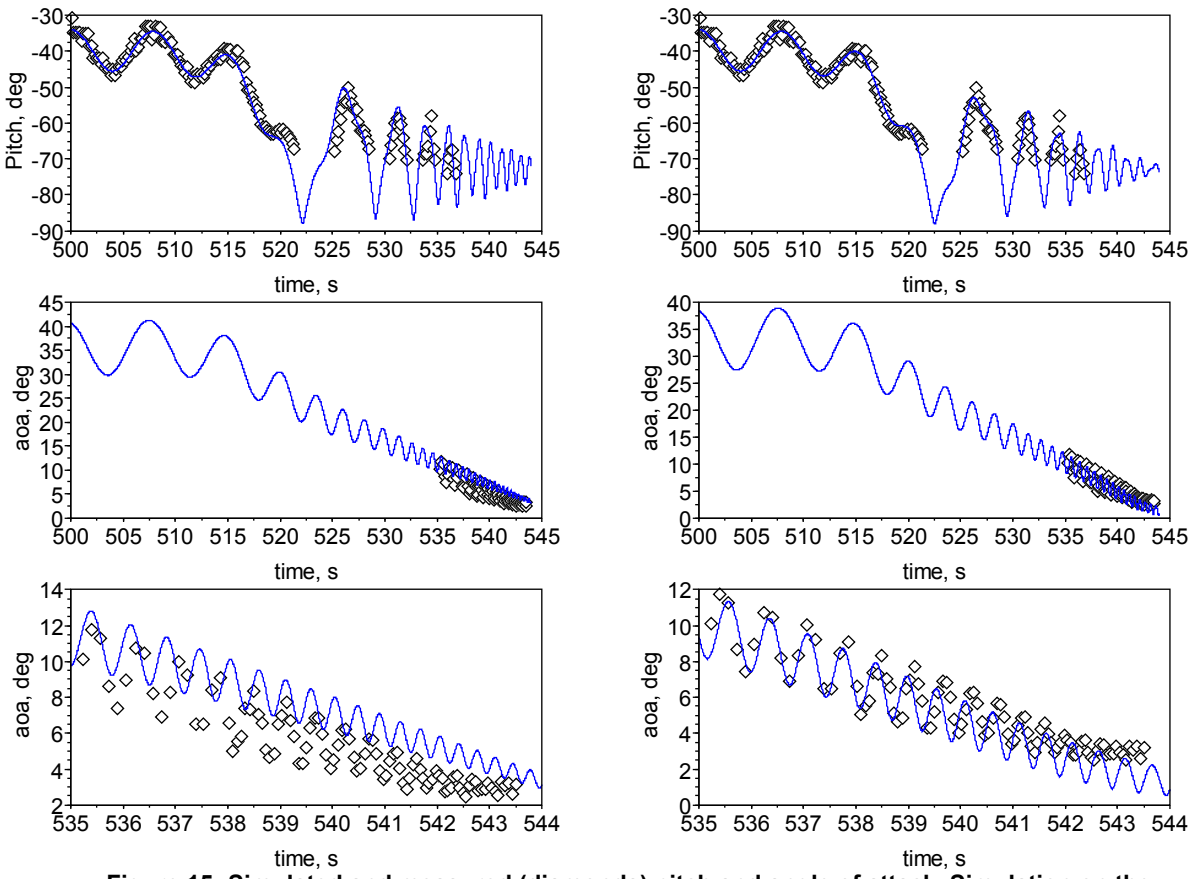

Figure 15: Simulated and measured (diamonds) pitch and angle of attack. Simulation on the right involves adjustment to aerodynamics and initial heading

Results are presented in figure 15 for simulations with and without adjustment to the initial heading and aerodynamics. The results of the "honest simulation" are not bad but replication of the flight data is greatly improved by: increasing C_{nr} by a factor of five, setting C_{mq} to zero; and increasing the initial vehicle heading by 10°. The adjustments to the aerodynamic derivatives are discussed in reference [1] and are not a topic for this lecture. Although a 10° error in heading is unlikely given the fidelity of the reorientation manoeuvre simulation, the primary effect of the adjustment is to reduce the initial angle of

attack from 41° to 39° and this is within the uncertainty of the pitch measurement. Although this uncertainty has not been quantified, it does increase as altitude decreases and the measurement becomes more sensitive to the height of the limb.

7 CONCLUSIONS

Most of the telemetry channels in Hyshot flights were dedicated to pressure measurements in the scramjet combustor. The vehicle state had to be determined from just seven onboard sensors: Three accelerometers; one horizon sensor; one magnetometer; and two Pitot probes. Although less than ideal, this instrumentation was sufficient to obtain a very good reconstruction of the flights, including the roll pitch resonance and resulting failure of Hyshot-1.

The flight tests and subsequent analysis were a lesson in flight dynamics for the author, and I would recommend to any aerodynamicist that he write a six degree of freedom trajectory code to get a better understanding of the significance of his aerodynamic output. If more aerodynamicists were doing flight simulations there would probably be significantly more work done on stability and dynamic derivatives.

Three general lessons from Hyshot that may help others planning a flight test are:

- After years of preparation for a test, the vehicle may disappear from view in seconds and never be seen again. Make sure that there are enough instruments on board and on the ground to give a reasonable chance of determining what went wrong even though this will probably be at the expense of the payload.

- As the test is being prepared, the vehicle and instrumentation are likely to develop and change. Prior to flight it is important to be sure that what is being tested is sufficiently well characterised. Dimensions, mass properties, and end-to-end instrumentation calibrations should be given a high priority pre-flight because they will probably be impossible post-flight.

- Having more than one method of deriving a quantity can help save the whole data set. The redundancy that this sometimes implies will probably come at the expense of payload, but it is better to have a limited quantity of good data than a large set of unusable data.

8 ACKOWLEDGEMENT

The author would like to thank Prof. Allan Paull at the University of Queensland for providing the flight data.

9 REFERENCES

[1] Cain T., Owen R., and Walton C., 2004, *Hyshot2 Aerodynamics*, 5th European Symposium on Aerothermodynamics for Space Vehicles, Cologne, Germany, 8-11 Nov. 2004.

[2] Owen R and Cain T., 2004, *Reconstruction of the Hyshot2 flight from onboard sensors,* 5th European Symposium on Aerothermodynamics for Space Vehicles, Cologne, Germany, 8-11 Nov. 2004.

[3] McMartin N, 2002, *Final Report of the Investigation into the anomaly of the HyShot Rocket at Woomera, South Australia on 30 October 2001*. Australian Transport Safety Bureau, SBN 0642 7 2210 2, 18 June 2002.

[4] Gainer T. and Hoffman S., 1972, *Summary of transformation equations and equations of motion used in free-flight and wind-tunnel data reduction and analysis*, NASA SP-3070.